




Multifunctional blazed gratings for multiband spatial filtering, retroreflection, splitting, and demultiplexing based on C_2 symmetric photonic crystals

Cite as: J. Appl. Phys. **131**, 223101 (2022); <https://doi.org/10.1063/5.0093989>

Submitted: 31 March 2022 • Accepted: 04 May 2022 • Published Online: 08 June 2022

 Andriy E. Serebryannikov,  Diana C. Skigin,  Guy A. E. Vandenbosch, et al.



View Online



Export Citation



CrossMark

Lock-in Amplifiers
up to 600 MHz



Zurich
Instruments



Multifunctional blazed gratings for multiband spatial filtering, retroreflection, splitting, and demultiplexing based on C_2 symmetric photonic crystals

Cite as: J. Appl. Phys. **131**, 223101 (2022); doi: [10.1063/5.0093989](https://doi.org/10.1063/5.0093989)

Submitted: 31 March 2022 · Accepted: 4 May 2022 ·

Published Online: 8 June 2022



View Online



Export Citation



CrossMark

Andriy E. Serebryannikov,^{1,a)} Diana C. Skigin,² Guy A. E. Vandebosch,³ and Ekmel Ozbay⁴

AFFILIATIONS

¹Division of Physics of Nanostructures, ISQI, Faculty of Physics, Adam Mickiewicz University, 61-614 Poznań, Poland

²Universidad de Buenos Aires, Facultad de Ciencias Exactas y Naturales, Departamento de Física, Grupo de Electromagnetismo Aplicado and CONICET-Universidad de Buenos Aires, Institute de Física de Buenos Aires (IFIBA), Buenos Aires, Argentina

³WaveCoRe Research Group, Electrical Engineering Department (ESAT), Katholieke Universiteit Leuven, 3001 Leuven, Belgium

⁴Nanotechnology Research Center (NANOTAM), National Institute of Nanotechnology and Materials Science (UNAM), Department of Physics, Department of Electrical Engineering, Bilkent University, 06800 Ankara, Turkey

^{a)}Author to whom correspondence should be addressed: andser@amu.edu.pl

ABSTRACT

The concept of multifunctional reflection-mode gratings that are based on rod-type photonic crystals (PhCs) with C_2 symmetry is introduced. The specific modal properties lead to the vanishing dependence of the first-negative-order maximum on the angle of incidence and the nearly sinusoidal redistribution of the incident-wave energy between zero order (specular reflection) and first negative diffraction order (deflection) at frequency variation. These features are key enablers of diverse functionalities and the merging of different functionalities into one structure. The elementary functionalities, of which multifunctional scenarios can be designed, include but are not restricted to multiband spatial filtering, multiband splitting, retroreflection, and demultiplexing. The proposed structures are capable of multifunctional operation in the case of a single polychromatic incident wave or multiple mono-/polychromatic waves incident at different angles. The generalized demultiplexing is possible in the case of several polychromatic waves. The aforementioned deflection properties yield merging demultiplexing with splitting in one functionality. In turn, it may contribute to more complex multifunctional scenarios. Finally, the proposed PhC gratings are studied in transmissive configuration, in which they show some unusual properties.

Published under an exclusive license by AIP Publishing. <https://doi.org/10.1063/5.0093989>

I. INTRODUCTION

Finite-thickness slabs of a photonic crystal (PhC), known as PhC diffraction gratings, started attracting interest more than a decade ago.^{1–4} PhC gratings and metamaterial based gratings, both having one-side corrugations, have been well known due to the structurally nonsymmetric designs enabling asymmetric transmission (AT). It is connected with one-way deflection that is yielded by the specific incident-wave energy redistribution in favor of higher diffraction order(s).^{5–7} Therefore, deflection serves as the main enabler of diverse functionalities in PhC gratings. The common

effect of dispersion of a Floquet–Bloch mode of the PhC and diffractions at the corrugated interfaces may enable a myriad of advanced functionalities. It is noteworthy that in the early-stage studies of the deflecting (blazed) gratings, the emphasis has been put on the operation at the Bragg condition.^{8–10} Later, this restriction has been mitigated in the advanced designs of the blazed gratings, including PhC gratings.^{11–14} Novel blazed gratings^{12,13,15} and recently proposed metasurfaces^{16,17} and meta-gratings¹⁸ are capable of deflection with a rather arbitrary choice of geometric parameters and angle of incidence.

Structures capable of *multifunctional operation* are trendy due to the prospective solutions offered for device miniaturization and system integration.^{18–20} Multifunctionality in PhC gratings assumes that different wave processes or groups of processes can be separated in space²¹ and/or in the frequency domain.⁵ The recently proposed metasurfaces offer multifunctional scenarios with either different functionalities or different manifestations of the same functionality in the neighboring frequency ranges,^{22–24} at different incidence angles,^{17,25} or for different polarization states.^{26–28} Two functionalities can be merged into one at a fixed frequency.^{29–32} The multifunctional scenarios that have been recently studied by numerous research groups include the elementary functionalities like focusing, deflection, polarization manipulation, splitting, and vortex and Bessel beam generation.

Very recently, periodic meta-arrays with wideband and simultaneously wide-angle deflection, which enable spatial filtering, wide-angle splitting, and other functionalities in one structure, have been demonstrated in the reflection mode.¹⁸ The earlier examples of PhC gratings with functionality integration include those yielding one-way splitting, spatial separation of two wave processes, and diodelike AT with opposite directions of strong transmission at two close frequencies.^{5,21,30} Examples of similar integration are also known for other configurations based on PhCs.^{23,33,34} Although metasurfaces can suggest electrically thinner performances than PhCs, it is still unclear whether they may replicate all functionalities achievable in PhCs or not. The diversity of modal properties of PhCs makes them a proper platform for multifunctional devices.

In the present paper, the concept of PhC gratings backed with a metallic reflector, which is capable of new multifunctional operation scenarios, is proposed and numerically validated. The goal of this study is the demonstration of multifunctional scenarios achievable due to the specific Floquet–Bloch mode of the PhCs. The desired modal properties can be obtained in the PhCs with a rectangular lattice, i.e., with the C_2 symmetry. Diffractions are achieved due to a larger lattice constant along the interface direction (i.e., $a_x > a_y$). The focus in this study is such multifunctional scenarios that are expected to be unachievable in the earlier proposed quasi-planar structures and PhC gratings. It will be demonstrated that (a) the incidence-angle insensitive -1 st-order deflection and (b) the frequency selective -1 st-order deflection together with the 0 th-order specular reflection enable multiband bandpass and band-stop spatial filtering, partial or full demultiplexing, and multiband splitting in one structure, within the same frequency range. Notably, spatial filtering,^{35–44} demultiplexing,^{45–49} and splitting^{50–56} belong to the basic functionalities that are commonly demanded in photonics, optical communications, etc. We will demonstrate how the aforementioned functionalities can be efficiently integrated into one structure. Moreover, multiband retroreflection and multiplexing can be obtained in the same structure and the same modal regime. This remains true for the generalized demultiplexing and for merging of demultiplexing and splitting functionalities into one functionality. The diffraction properties of the proposed PhC grating but without a reflector will also be discussed.

It is noteworthy that, despite some of the aforementioned elementary functionalities that can be obtained in structures of other types, low-symmetric PhCs are used here to enable *all* or

most of the required elementary functionalities at a given frequency range in one device, according to the purposes of this study. For instance, some demultiplexing scenarios might be obtained by using volume Bragg gratings.^{57,58} However, it can then be a challenge to obtain multiband spatial filtering, like that proposed in this paper, in the same structure and at the same frequency range. To calculate reflectance and transmittance, the coupled integral equations technique with controllable accuracy and convergence has been used.⁵⁹ Since the general dispersion properties of PhCs with C_2 symmetry are known, a study of dispersion is beyond the scope of this paper. It is organized as follows. The Geometry and Methods section (Sec. II) follows the Introduction (Sec. I). It is followed by the Results and Discussion section (Sec. III) that is divided into three subsections dedicated to multiband spatial filtering and retroreflection, partial and generalized demultiplexing and multiband splitting, and PhC gratings without a reflector. Then, a short Conclusion is presented (Sec. IV).

II. GEOMETRY AND METHODS

The general geometry of the proposed grating is shown in Fig. 1. It represents a finite-thickness slab of PhC with C_2 symmetry that is placed above the metallic reflector. Structures of this type of symmetry are known for self-collimation and other fascinating propagation effects.^{50,60–64} In this context, the canalization

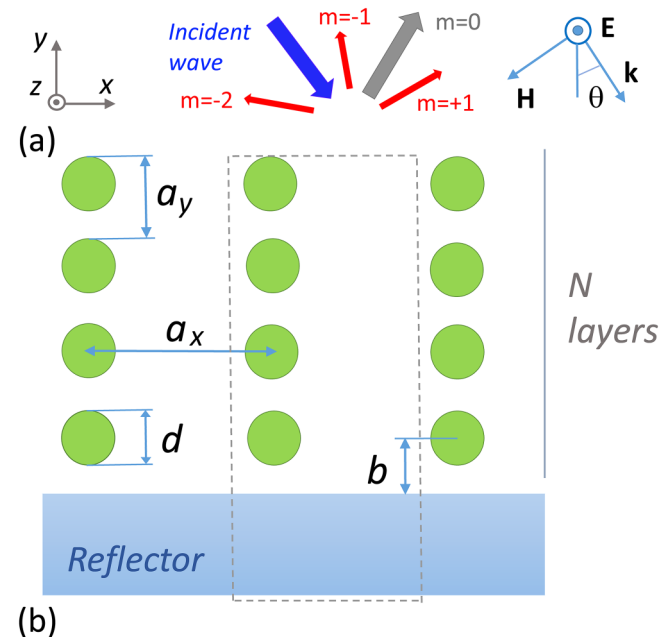


FIG. 1. (a) From left to right: the used coordinate system, schematic of directions of the incident and diffracted waves in case when the orders $m = 0, -1, -2,$ and $+1$ are propagating, orientation of the field vectors (\mathbf{E} and \mathbf{H}), and wavevector (\mathbf{k}) and definition of incidence angle (θ). (b) General geometry of the studied PhC grating with back-side reflector, $a_x = 2a_y = L$. Three periods over x are shown. Dashed gray frame shows the calculation region.

of electromagnetic waves should also be mentioned.⁶⁵ The studied structure is assumed to be periodic and infinitely long in the x direction. It is illuminated from the upper half-space by a linearly polarized plane wave incident obliquely at angle θ . Consideration is restricted to TE polarization, i.e., the electric field vector is parallel to the z axis. The rods are assumed to be made of a dielectric material with relative permittivity ϵ_r . The x and y components of the PhC lattice vector components are denoted by a_x and a_y , respectively; here, $a_x = 2a_y$. Thus, the grating period L is equal to a_x . The ratio $d/a_y = 0.4$, where d is the rod diameter, is used throughout the paper. For instance, at $L = a_x = 1.5\ \mu\text{m}$, we have $a_y = 750\ \text{nm}$ and $d = 300\ \text{nm}$. Other values of d/a_y have also been examined. The only requirement for the back-side reflector is that it should be weakly absorptive and weakly transmissive. It is achieved for a very wide variety of materials and geometrical parameters. For the sake of definiteness, it is assumed here that the reflector is made of a Drude metal with permittivity $\epsilon_m = 1 - \omega_p/[\omega(\omega - i\gamma)]$, where ω_p is the angular plasma frequency and γ is the angular collision frequency; $\omega_p a_y/c = 20\pi$ and $\gamma/\omega_p = 0.01$. The host medium is assumed to be air.

The incident wave is given by

$$E^i(x, y) = E_0 \exp(i\alpha_0 x - i\beta_0 y), \quad (1)$$

where E_0 is the amplitude, $\alpha_0 = k \sin \theta$, $\beta_0 = k \cos \theta$, $k = \omega/c$ is the free-space wavenumber, $\omega = 2\pi f$ is the angular frequency, f is the frequency, and c is the speed of light in vacuum. The electric field above the PhC grating is presented as follows:

$$E^+(x, y) = E^i(x, y) + \sum_{m=-\infty}^{\infty} \rho_m \exp(i\alpha_m x + i\beta_m y), \quad (2)$$

where $\beta_m = \sqrt{k^2 - \alpha_m^2}$, $\text{Im} \beta_m \geq 0$, $\alpha_m = \alpha_0 + 2\pi m/L$, and ρ_m is the amplitude of the m th-order reflected wave. The transmitted electric field below the reflector is given by

$$E^-(x, y) = \sum_{m=-\infty}^{\infty} \tau_m \exp(i\alpha_m x - i\beta_m y), \quad (3)$$

where τ_m is the amplitude of the m th-order transmitted wave. For a reflective configuration, E^- can be near zero at the appropriate choice of material and thickness of the reflector. However, it is nonzero in the general case, i.e., when the reflector is semi-transparent or removed.

The coupled integral equation technique is used for the purposes of numerical study. The used technique is based on the standard conversion of the frequency-domain Maxwell equations into the electric-field integral equation⁶⁶ and, further, into a set of the coupled integral equations with respect to the y -dependent amplitudes of the individual space harmonics (diffraction orders). Finally, these equations are discretized by considering a finite number of points over y axis, i.e., from the top of the PhC to the bottom of the reflector. This leads to the set of algebraic equations with respect to the amplitudes of the electric field for the individual space harmonics at the selected values of y . It is solved with controllable convergence and accuracy by using the fast iterative algorithm, whose details can be found in Ref. 59.

Once the amplitudes at the upper and lower boundaries of the calculation region are found, the values of ρ_m and τ_m , including those at $m = 0$ and $m = -1$, are directly calculated. Throughout the paper, we use m th-order reflectances, $r_m = \rho_m \rho_m^* \text{Re} \beta_m / W$, and m th-order transmittances, $t_m = \tau_m \tau_m^* \text{Re} \beta_m / W$, in order to quantify far-field behavior. Here, W is the energy of the incident wave and an asterisk means a complex conjugate. In the loss-free case, $R + T = W$, where $R = \sum_{m=-\infty}^{\infty} r_m$ is the overall reflectance and $T = \sum_{m=-\infty}^{\infty} t_m$ is the overall transmittance. In the reflective configuration, $T \approx 0$.

The angle of the m th-order outgoing wave can be found from the grating equation,⁶⁷

$$\sin \phi_m = \sin \theta + 2\pi m/kL, \quad (4)$$

where $m = 0, \pm 1, \pm 2, \dots$; ϕ_m and θ are measured, respectively, in the clockwise and the counterclockwise direction from the y axis; and kL represents the normalized frequency. The structure can be designed so that a desired number of the diffraction orders may propagate, while the remaining ones are evanescent. In our PhC gratings, the orders $m = 0$ and $m = -1$ are propagating, whereas the ones with $m > 0$ and $m < -1$ are evanescent. In this case, $R = \sum_{m=-1}^0 r_m$ and $T = \sum_{m=-1}^0 t_m$.

As follows from the obtained results (which will not be shown), the used aspect ratio of $a_x/a_y = 2$ is optimal for the required sinusoidal distribution of the incident-wave energy between the orders $m = 0$ and $m = -1$ within a wide f -range. One of the reasons to use this value of a_x/a_y is the intention to match the ka_x -range wherein the Floquet–Bloch mode assuring a weak dependence of reflection at $m = -1$ on θ co-exists with the ka_x -range wherein only the orders $m = 0$ and $m = -1$ are propagating.

III. RESULTS AND DISCUSSION

A. Multiband spatial filtering and retroreflection

In this section, we demonstrate the potential of the proposed structures based on C_2 symmetric PhCs in multiband spatial filtering and retroreflection. These functionalities belong to a set of elementary functionalities, which serve as the building blocks for multifunctional operation scenarios. For plane-wave illumination, spatial filtering represents an analog of frequency-domain filtering but in the θ -domain, while $f = \text{const}$ (see Ref. 35). Various mechanisms and structures have been proposed for reflection and transmission modes that enable low-pass, bandpass, and bandstop spatial filtering. Compared to the other designs of PhCs and meta-gratings that enable spatial filtering in reflection mode at plane-wave illumination,^{15,18,68} a few periods of the PhC along the y axis are considered in our study. This difference is crucial for obtaining multiple regions of $r_{-1} \approx 1$ in (kL, θ) -plane, which are intermittent with the regions of $r_0 \approx 1$ (i.e., small r_{-1}) and weakly dependent on θ . It assures multiple widebands of spatial filtering, in line with the purposes of this work, while the use of one period over the y axis assures the appearance of a rather large but a single region of $r_{-1} \approx 1$, as shown in Refs. 15 and 18. The same is expected to be true for the structures studied in Ref. 68, in which the emphasis has been put on other spectral and operation regimes and other

aspects of spatial filtering. In particular, we use the range of smaller L/λ (λ is wavelength), i.e., $0.5 < L/\lambda < 1$, whereas the orders $m = -1$ and $m = 0$ are the main enablers of the resulting functionality. Notably, at beam illumination, the contribution of the individual angular components is modified so that the beam *reshaping* takes place (e.g., see Refs. 68 and 69). Such regimes are beyond the scope of the present paper.

The results for the first-negative-order reflectance, r_{-1} , vs kL are presented in Fig. 2. The “mountains” of $r_{-1} \approx 1$ and “valleys” of small r_{-1} are the main features observed here. At the “mountains,” almost total conversion of the incident-wave energy into a deflected beam outgoing at the angle ϕ_m takes place. The “valleys” of small r_{-1} correspond to the “mountains” of r_0 (not shown), while the transmission is negligible. From the spatial filtering

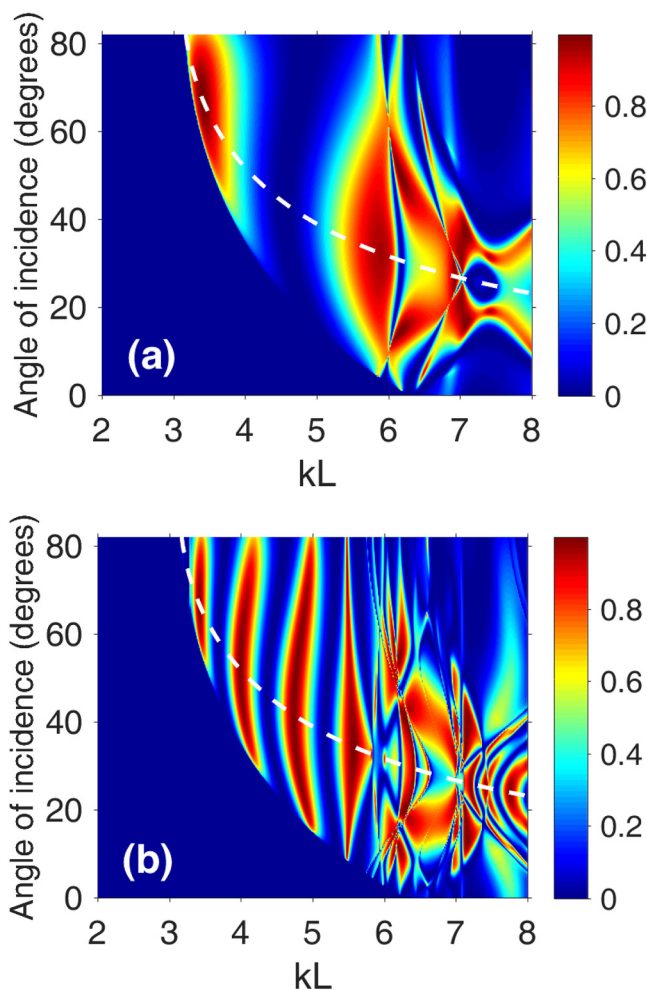


FIG. 2. First-negative-order reflectance, r_{-1} , at the simultaneous variation of kL and θ for the PhC grating with (a) $N = 2$, (b) $N = 6$, $\epsilon_r = 11.4$; the grating is backed with a metallic reflector. Dashed white lines correspond to the retroreflection regime, in which $\phi_{-1} = -\theta$.

perspective, it is important that we have non-bent “mountains,” i.e., the spectral location of the maxima of r_{-1} should not be strongly changeable at variations of θ in a wide range. This behavior corresponds to the flat dispersion occurring within a wide but limited range of wavenumber variation. It indicates, among others, the principal possibility of a nearly sinusoidal energy exchange between r_0 and r_{-1} when f is varied, and the fact that the exchange scenario can weakly depend on θ .

The regimes of $r_{-1} \approx 1$ enable multiband bandpass filtering in the θ -domain. The complementary regions of $r_0 \approx 1$ that occur in the same spectral regimes but for smaller θ yield bandstop filtering. The effect of N manifests itself in the different numbers of the intermittent regions of $r_0 \approx 1$ and $r_{-1} \approx 1$. There are two regions of large r_{-1} near $kL = 3.4$ and 5.9 in Fig. 2(a), and four such regions around $kL = 3.42, 4.0, 4.75,$ and 5.55 in Fig. 2(b). Interestingly, similar features have been observed for transmission-mode spatial filtering in diffraction-free PhCs, where the intermittence occurs for t_0 and r_0 .³⁵ In our case, the reflected order r_{-1} plays the same role in spatial filtering as t_0 does in Ref. 35.

Note that ϕ_{-1} may vary in a very wide range within each “mountain.” For instance, at $kL = 5.486$, we obtain $\phi_{-1} = -81.4^\circ$ at $\theta = 9^\circ$ and $\phi_{-1} = -8.9^\circ$ at $\theta = 82^\circ$, in agreement with the Lorentz reciprocity. Clearly, the continuous variation of ϕ_{-1} from -81.4° to -8.2° occurs when θ is continuously varied from 9° to 82° . At $kL = 4.05$, we obtain $\phi_{-1} = -71^\circ$ at $\theta = 37^\circ$ and $\phi_{-1} = -38.2^\circ$ at $\theta = 68^\circ$. Such wide ranges of the output-wave angle make the multiband *retroreflection* regime possible that is achieved when $\phi_{-1} = -\theta$ and $\sin \phi_{-1} = -\pi/kL$.^{70–72} This regime is known as Littrow mounting. As observed in Fig. 2, retroreflection occurs within each “mountain” so that the number of the retroreflection bands depends on N . In particular, retroreflection is observed at $\theta = 51^\circ$ when $kL = 4.05$, and at $\theta = 34.9^\circ$ when $kL = 5.486$. Moreover, the neighboring kL -ranges corresponding to another Floquet–Bloch mode (e.g., $6 < kL < 8$) may also contribute to the resulting multiband retroreflection. Interestingly, we obtain $r_{-1} > 0.9$ for $\phi_{-1} = -\theta$ when not only the orders $m = 0$ and $m = -1$ but also the order $m = -2$ may propagate according to Eq. (4). The demonstrated multiband retroreflection differs from wideband retroreflection in Ref. 18 because the former may need the well adjusted values of kL and θ .

For more evidence, Fig. 3 presents r_0 and r_{-1} at the selected values of kL , which correspond to the tops of the “mountains” in Fig. 2(b). As observed, we obtain bandstop spatial filtering for r_0 and bandpass spatial filtering for r_{-1} . It is seen that $r_{-1} > 0.9$ in a wide θ -range. The boundaries of the θ -domain bands are moderately sharp, and the upper- θ boundary is more blurred than the lower one. The width and location of the θ -domain band depend on which “mountain” is chosen. The location of the lower- θ boundary in Fig. 3(b) can vary from $\theta = 10^\circ$ to 60° , depending on the choice of kL -value. You can see that the band widening is possible at the price of a decrease of $\max r_{-1}$ and a less smooth shape of r_{-1} vs θ ; compare the cases of $kL = 5.486$ and $kL = 5.546$ in Fig. 3(b). This remains true for all four “mountains.” The features observed in Figs. 2 and 3 can be obtained for various rod materials, e.g., those with $5.6 < \epsilon_r < 12.5$. As shown in Sec. III B, partial and generalized demultiplexing scenarios and multiband splitting can be obtained in the same structure and at the same frequency range as

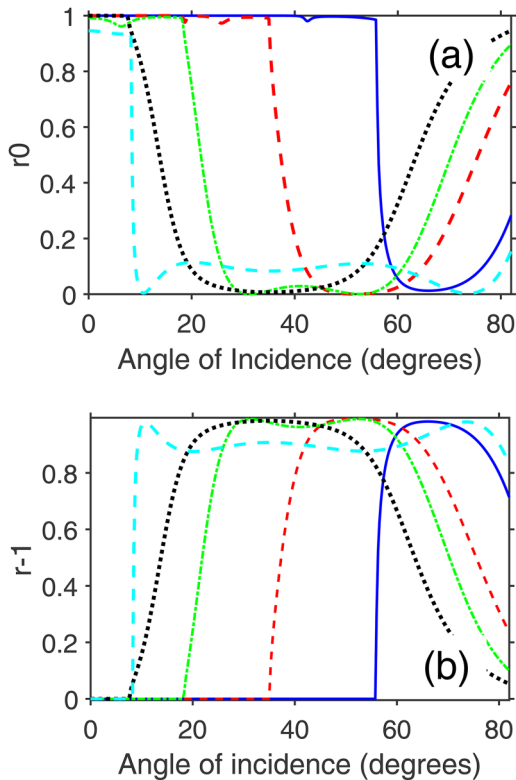


FIG. 3. (a) Zero-order reflectance, r_0 , and (b) first-negative-order reflectance, r_{-1} , as a function of θ for the same structure as in Fig. 2(b). Solid blue, dashed red, dash-dotted green, dashed cyan, and dotted black lines correspond to $kL = 3.434, 3.99, 4.783, 5.486,$ and 5.546 , respectively.

multiband spatial filtering and retroreflection. No additional parameter adjustment is needed. This makes the proposed PhC gratings highly capable in multifunctional operation.

B. Partial and generalized demultiplexing and multiband splitting

In this section, we demonstrate the potential of the designed PhC gratings in *demultiplexing* and *multiband splitting*, which represents the second part of the selected elementary functionalities. Figure 4 presents zero-order and first-negative-order reflectance, r_0 and r_{-1} , vs kL for a grating created by a finite-thickness slab of PhC with C_2 symmetry, which is backed by a metallic reflector. Structures with different numbers of rod layers, N , were compared. As expected, the nearly sinusoidal energy exchange between the orders $m = 0$ and $m = -1$ occurs at varying frequencies. Notably, this feature is rather uncommon for PhCs because it needs specific modal properties and geometrical parameters. For the energy exchange of such a kind, the maxima of $r_{-1} \approx 1$ ($m = -1$, $\phi_{-1} \neq -\theta$) are intermittent with the specular reflection regimes of $r_0 \approx 1$ ($\phi_0 = \theta$), when $3.8 < kL < 5.7$, in agreement with Fig. 2. The number of the reflection regimes of each of the two types

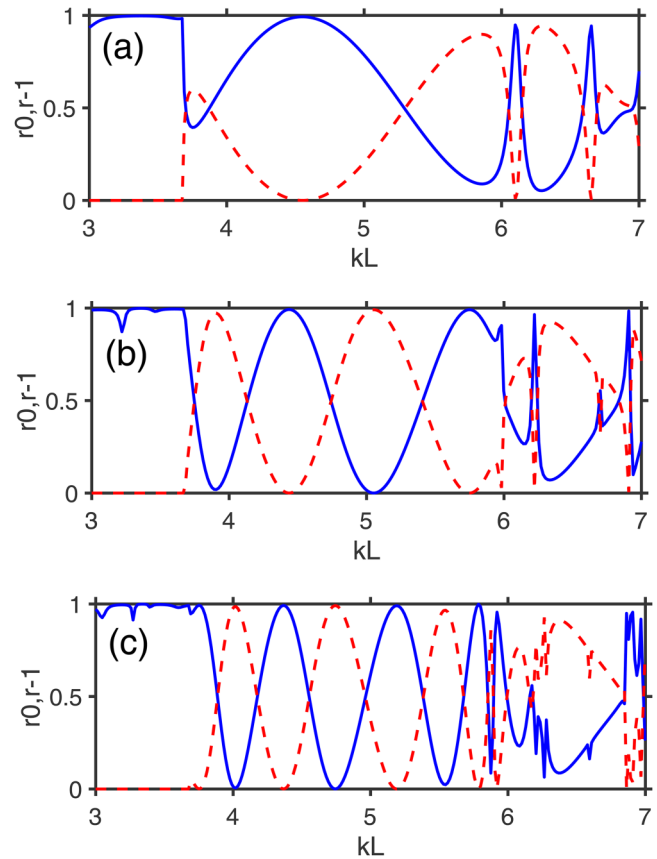


FIG. 4. Reflectance vs kL for PhC grating with (a) $N = 2$, (b) $N = 4$, (c) $N = 6$, $\epsilon_r = 11.4$, $\theta = 45^\circ$; the grating is backed with a reflector; solid blue line— r_0 , dashed red line— r_{-1} .

depends on N [compare Figs. 4(a)–4(c)]. For $N = 2$, we have one reflection region with $r_0 \approx 1$ and one region with $r_{-1} \approx 1$. For $N = 4$, there are two regimes of $r_{-1} \approx 1$ and two regimes of $r_0 \approx 1$ within the same kL -range. For $N = 6$, there are three regimes of $r_{-1} \approx 1$ and three regimes of $r_0 \approx 1$.

The observed intermittence reminds us about Fabry–Pérot interferences in a finite-thickness slab of a homogeneous dielectric material. The difference is that now we have r_0 and r_{-1} instead of r_0 and t_0 . Figure 5 presents electric field distribution within one period of the structure along the x axis. The chosen values of kL correspond to the maxima of $r_0 \approx 1$ and $r_{-1} \approx 1$ in Fig. 4(c). Figures 5(a), 5(c), and 5(e) correspond to $r_{-1} \approx 1$; Figs. 5(b) and 5(d) correspond to $r_0 \approx 1$. The observed features give evidence of the interferential nature of the mechanism of energy exchange between the orders $m = 0$ and $m = -1$. Here, the equivalent grating thickness $D \approx \lambda_{\text{PhC}}/2$ is needed to obtain $r_0 \approx 1$, while $D \approx \lambda_{\text{PhC}}/4 + l\lambda_{\text{PhC}}/2$ leads to $r_{-1} \approx 1$ (λ_{PhC} is the wavelength in the PhC along the y direction, l is an integer). These two conditions for D correspond to the constructive and destructive interferences in a non-backed homogeneous dielectric slab. The former leads to

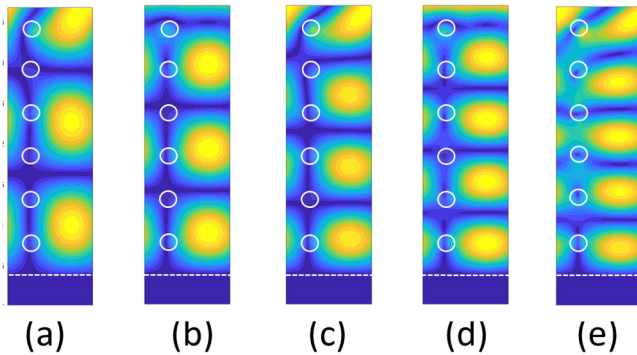


FIG. 5. Examples of the electric field distribution within one period over x at $N = 6$, $\epsilon_r = 11.4$, $\theta = 45^\circ$; (a) $kL = 4.01$, (b) 4.37, (c) 4.75, (d) 5.19, and (e) 5.54. Local field maxima are observed at the mid-distance between the neighboring rods in x direction. The dashed white line indicates the upper surface of the metallic reflector.

$t_0 = 1$ and the latter to a maximum of r_0 . Compared to Ref. 68, Mie resonances of individual rods do not contribute to the resulting physical mechanism. Note that various effects of interferences have earlier been studied in PhCs of different types.^{5,73,74} On the other hand, the observed features may remind a *Gires-Tornouis interferometer*. However, in contrast with its conventional theoretical model, we utilize here the orders $m = 0$ and $m = -1$ together with the specific modal properties that enable the desired multifunctional scenarios.

The observed behavior of r_0 and r_{-1} in Fig. 4 and that of r_{-1} in Fig. 2 indicate the principal possibility of *partial demultiplexing*, as illustrated by the schematic in Fig. 6. Let the wave incident at a given angle θ represents a polychromatic wave comprising several

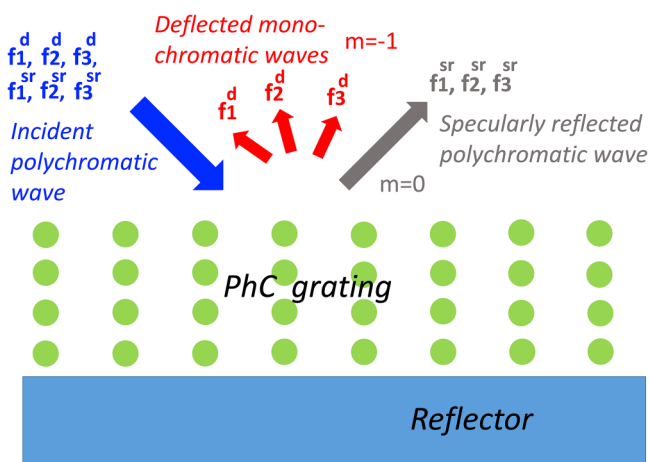


FIG. 6. Schematic illustrating the merging of partial demultiplexing and splitting functionalities for a single polychromatic wave incident at given θ , in line with Eq. (5). In this example, it is assumed that $P = 3$ and $Q = 3$.

spectral components. They correspond to (nearly) perfect deflection, $r_{-1} \approx 1$ (frequencies $f_1^d, f_2^d, \dots, f_p^d$), and several spectral components corresponding to the specular reflection regime, $r_0 \approx 1$ (frequencies $f_1^{sr}, f_2^{sr}, \dots, f_Q^{sr}$), i.e., the incident wave is given as follows:

$$u(t, \mathbf{r}) = \sum_{p=1}^P A_p \exp(-i2\pi f_p^d t + i\mathbf{k}\mathbf{r}) + \sum_{q=1}^Q A_q \exp(-i2\pi f_q^{sr} t + i\mathbf{k}\mathbf{r}), \quad (5)$$

where A_p and A_q are the amplitudes, \mathbf{k} is the wave vector, and \mathbf{r} is the generalized coordinate.

Then, the components with $f = f_p^d$ will be deflected, creating monochromatic deflected waves. The kL -dependent angles ϕ_m are given by Eq. (4) with $m = -1$. In turn, all of the components with $f = f_q^{sr}$ will be specularly reflected so that a new polychromatic wave will be formed. In such a way, the first part of the incident wave is demultiplexed, while the second part is not. Clearly, the demultiplexed (deflected) and nondemultiplexed (specularly reflected) parts are forwarded to the different regions of the upper half-space, as shown in Fig. 6. Notably, they can be forwarded even to different quadrants. Thus, the discussed functionality can also be understood in the context of *sorting*, i.e., separation of the spectral components of the incident wave by redirecting them to different angular sectors or different quadrants. For instance, for the regimes of $r_{-1} \approx 1$ in Fig. 4(c), we obtain $\phi_{-1} \approx -59^\circ, -38^\circ$, and -25° , respectively, at $kL = 4.01, 4.75$, and 5.54 , while $\phi_0 = 45^\circ$ for the regimes of $r_0 \approx 1$. Besides, the incident wave can be either a superposition of monochromatic waves with only $f = f_i^d$ or only $f = f_i^{sr}$ [see Eq. (5)]. Then, in the former case, we obtain a full demultiplexing, i.e., all spectral components are deflected to the different values of ϕ_{-1} . In the latter case, we obtain conventional specular reflection. The retroreflection regime can be excluded from the set of the outgoing waves.

The same structures suggest *multiband splitting* when $r_0 = r_{-1} \approx 0.5$. Let us reconsider the case of a polychromatic incident wave that represents a superposition of monochromatic waves with different f , for each of which splitting may occur (frequencies $f_1^{sp}, f_2^{sp}, \dots, f_S^{sp}$), i.e.,

$$u^{sp}(t, \mathbf{r}) = \sum_{s=1}^S A_s \exp(-i2\pi f_s^{sp} t + i\mathbf{k}\mathbf{r}), \quad (6)$$

where A_s is the amplitude. Then, the splitting and demultiplexing functionalities can be *merged* in one step. In other words, half of the polychromatic incident wave energy is converted into a specularly reflected wave, and the other half is demultiplexed. In Fig. 4(c), it happens for $\phi_{-1} \approx -65^\circ, -53^\circ, -42^\circ, -34^\circ, -27^\circ, -23.5^\circ$, and -21.5° , respectively, at $kL = 3.89, 4.18, 4.55, 4.97, 5.39, 5.68$, and 5.85 . In addition, none of the regimes of $r_{-1} \approx 1$ correspond to the Bragg condition. Moreover, the polychromatic incident wave may represent a sum of the components with f_q^{sr}, f_p^d , and f_s^{sp} . Then, an even more complex multifunctionality can be obtained. It is noteworthy that the full demultiplexing can also be obtained in reflective

quasi-planar meta-arrays like the ones in Refs. 15 and 18. However, it is achieved therein for a single wideband of large r_{-1} . Therefore, some of the selected elementary functionalities, i.e., partial demultiplexing and multiband splitting, are not achievable in that case.

Partial demultiplexing and multiband splitting can be tuned in the simplest way (i.e., without tunable materials) by varying θ . Since both ϕ_{-1} and the kL threshold for $|\sin \phi_{-1}| \leq 1$ depend on θ [see Eq. (4)] the width of the ϕ_{-1} range that is achievable in the used energy exchange regime can be varied with θ . The weak dependence of kL -values corresponding to the maxima of r_{-1} on θ , like that observed in Fig. 2(b), makes the generalization of demultiplexing possible, for which several polychromatic waves (instead of one polychromatic incident wave like in the case shown in Fig. 6) are incident at different angles, each comprising multiple spectral components [like in Eq. (5) for one polychromatic wave]. At the same time, the merging of partial demultiplexing and splitting functionalities may be obtained for each of such waves. Such generalization is difficult to obtain when using structures of other types, e.g., volume Bragg gratings.

The possibility of demultiplexing in the framework of this scenario is confirmed by the results in Fig. 7 for the PhC grating with $\varepsilon_r = 9.6$. Figure 7(a) presents r_0 and r_{-1} vs kL at $\theta = 45^\circ$. The results are similar to those in Fig. 4, in accordance with the fact that the observed energy exchange between the orders $m = 0$ and $m = -1$ takes place in a wide range of ε_r variation, e.g., from 5.6 to 12.5. Next, Fig. 7(b) shows r_{-1} vs kL for four selected values of θ . The intermittence of the maxima of $r_{-1} \approx 1$ and $r_0 \approx 1$ is the feature common for all values of θ [see Fig. 2(b) for comparison].

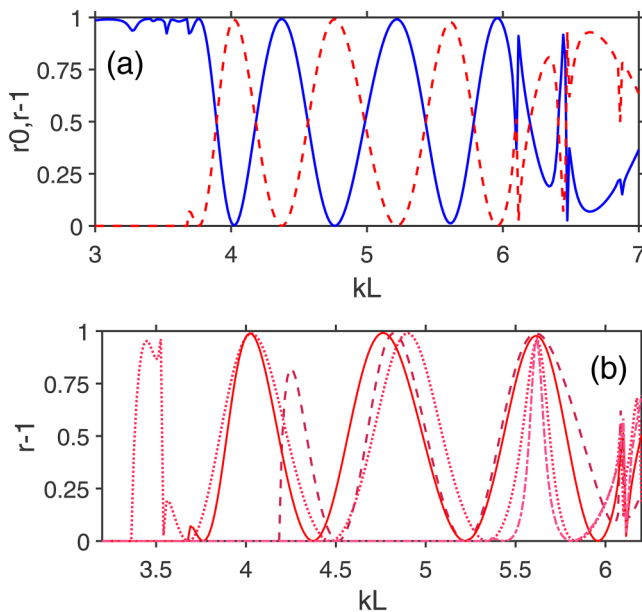


FIG. 7. Reflectance vs kL for the PhC grating with $\varepsilon_r = 9.6$ and $N = 6$; (a) solid blue line— r_0 , dashed red line— r_{-1} ; $\theta = 45^\circ$; (b) r_{-1} ; solid line— $\theta = 45^\circ$, dashed line— $\theta = 30^\circ$, dotted line— $\theta = 60^\circ$, dashed-dotted line— $\theta = 10^\circ$; a reflector is placed on the back side.

Maxima of r_{-1} of two types can be distinguished in Fig. 7(b). For the first one, spectral locations are the same for the maxima that correspond to different θ ; for the second one, spectral locations are slightly different. Nevertheless, they both may contribute to the demultiplexing scenarios, in which several polychromatic waves are incident at different angles. For instance, in the case shown in Fig. 7(b), we obtain $\phi_{-1} = -58.9^\circ$ and -44.2° , respectively, at $\theta = 45^\circ$ and 60° for $kL = 4.02$; $\phi_{-1} = -52.7^\circ$, -36° , and -25.4° at $\theta = 30^\circ$, 45° , and 60° for $kL = 4.85$; and $\phi_{-1} = -70.8^\circ$, -38.2° , -24.3° , and -14.6° at $\theta = 10^\circ$, 30° , 45° , and 60° for $kL = 5.62$. By adjusting the structural parameters and choosing proper values of θ , a difference in the achieved values of ϕ_{-1} can be obtained. On the other hand, an adjustment may lead to the case when two or more incident waves with different pairs of (kL, θ) are deflected to the same direction so that multiplexing/beam combining takes place. Clearly, not only conventional but also generalized demultiplexing can be a part of the complex multifunctional scenarios along with spatial filtering, retroreflection, and/or splitting. It is noteworthy that multiband spatial filtering and merging of (generalized) demultiplexing with splitting in one

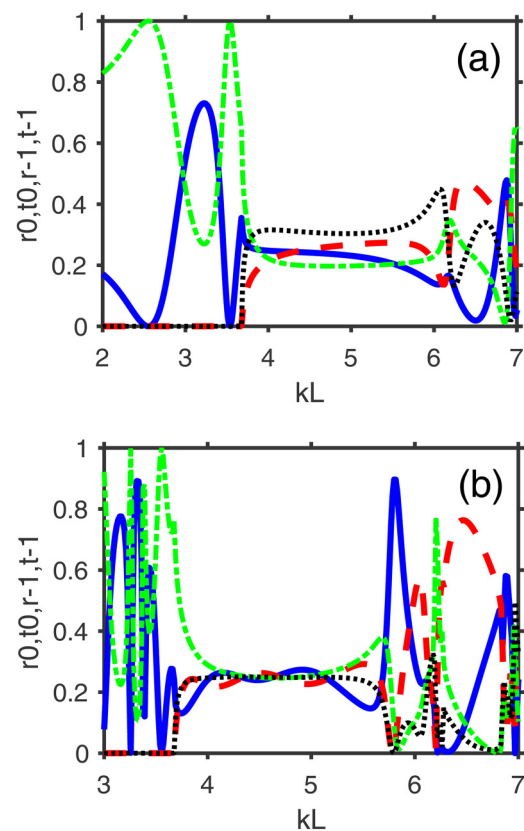


FIG. 8. Zero-order reflectance, r_0 (blue solid line), first-negative-order reflectance, r_{-1} (red dashed line), zero-order transmittance, t_0 (green dashed-dotted line), and first-negative-order transmittance, t_{-1} (black dotted line) vs kL , at (a) $N = 2$ and (b) $N = 6$; $\varepsilon_r = 11.4$, $\theta = 45^\circ$; there is no back-side reflector.

functionality cannot be obtained in the reflective structures with one period over the y axis that were studied in Refs. 15 and 18. The functionalities enabled by the sinusoidal redistribution of the incident-wave energy between the orders $m = 0$ and $m = -1$ invoke a few periods of the PhC over the y axis.

C. PhC grating without a reflector

In this section, we briefly discuss the transmission properties of the designed PhC gratings. The structure studied here is easily obtained from the basic geometry in Fig. 1 by removing the back-side reflector. Figure 8 presents the results for r_0 , r_{-1} , t_0 , and t_{-1} for the PhC grating with the same parameters as in Figs. 2, 3, 4(a), and 4(c). The most interesting feature here is that all four diffraction efficiencies vary weakly in the kL -range, in which we observed the energy exchange between -1 st and 0 th orders in the case with the reflector. Moreover, their values are close to each other for $N = 6$, say, at $4.2 < kL < 5.2$ ($-52^\circ < \phi_{-1} < -30^\circ$), and that enables a four-beam wideband splitter.

Finally, Fig. 9 presents the maps of t_{-1} and r_{-1} in (kL, θ) -plane. As observed, the features initially found in Fig. 8 remain the same within the large region, although t_{-1} varies weaker with kL and/or θ than r_{-1} does. Thus, the nearly equal efficiencies are not a result of

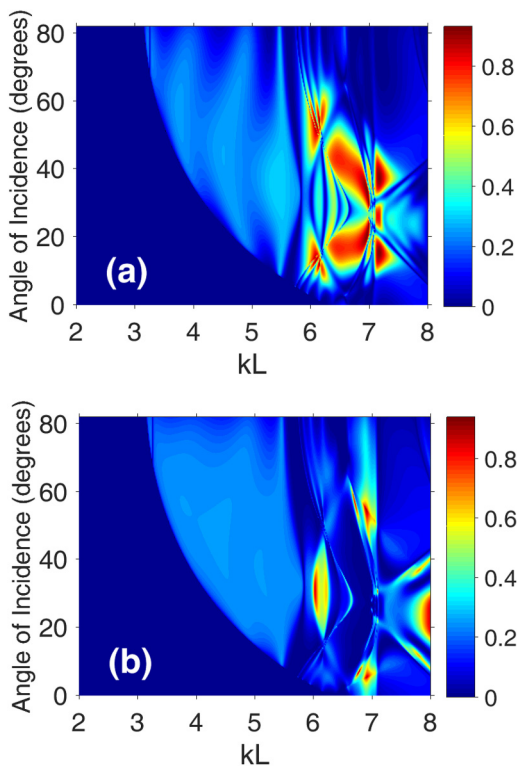


FIG. 9. (a) First-negative-order reflectance, r_{-1} , and (b) first-negative-order transmittance, t_{-1} , at simultaneous variation of kL and θ ; $N = 6$, $\epsilon_r = 11.4$; there is no back-side reflector.

an accidental choice of θ and kL . Rather, it reflects the nature of the used modal regime. It is noteworthy that a similar behavior has been observed in a wide range of ϵ_r variation, e.g., for $5.6 < \epsilon_r < 12.5$ (results are not shown). Interestingly, the behavior of r_0 , r_{-1} , t_0 , and t_{-1} outside the range $3.8 < kL < 5.7$ is completely different. It results from the difference in the properties of Floquet–Bloch modes inside and outside this range. Their analysis is beyond the scope and can be a subject of a future study.

IV. CONCLUSION

We studied the PhC gratings backed with a reflector that are capable of multifunctional operation so that several functionalities can be achieved in one structure, in the same frequency range. The specific modal properties that result from the C_2 symmetry of the used PhCs yield co-existence of angle-independent deflection and specific energy exchange between zero and first negative orders while varying frequency. They serve as the main enablers of the multifunctional scenarios. Therefore, there may be no full analog of the combination of functionalities proposed in the earlier works. The two aforementioned features are kept within a large region in (kL, θ) -plane. This allows you to select proper widths of the passbands in the θ -domain and achieve quite a large angular difference between the individual demultiplexed (outgoing) waves. One of the most interesting manifestations is probably the nearly perfect, multiband, wide-angle deflection occurring in the first negative diffraction order regime enabling multiband bandpass filtering in the θ -domain. Up to three spectral regimes of the nearly ideal deflection that are robust to the θ variations and intermittent with the spectral regimes of specular reflection have been numerically demonstrated. Notably, the energy exchange between the propagating zero and first negative orders in reflection is similar to that between reflectance and transmittance in the case of the interferences in a homogeneous transmissive dielectric slab. A larger number of the bands within the given frequency and/or incidence-angle ranges can be obtained by an increase in the number of rod layers. A polychromatic incident wave can experience either full or partial demultiplexing, or specular reflection, depending on which spectral components are comprised. The generalization of demultiplexing for the case of several polychromatic waves incident at different angles is proposed. It constitutes an important extension to multifunctional scenarios. A multiband splitter is one more functionality enabled by the peculiar first-negative-order deflection in the same frequency range. Moreover, demultiplexing and splitting functionalities can be merged into one functionality. The same PhC gratings can function as a multiplexer or a multiband retroreflector. On the other hand, it can be used just for a single functionality, if required. When the back-side reflector is removed, nearly equal efficiencies for all four propagating orders (zero and first-negative orders in transmission and reflection) are obtained. The use of both orthogonal polarizations can further reinforce the potential of multifunctionality. The studied structures can be appropriate for fabrication, since fabrication techniques for two-dimensional PhCs are well developed.^{75,76} The concept transfer to the PhC slabs will be considered in the next steps of this research program. The obtained results are important, first of all, from the multifunctionality perspective. They may be useful for the development of new near- and

far-infrared devices with a high degree of miniaturization and integration and indicate a route to new applications for low-symmetric PhCs and PhC gratings.

ACKNOWLEDGMENTS

This work was supported by the Narodowe Centrum Nauki (Project Nos. UMO-2015/17/B/ST3/00118 and UMO-2020/39/I/ST3/02413), TUBITAK (Program No. 2221), and projects UBACyT 20020150100028BA, UBACyT 20020190100108BA, and CONICET PIP 11220170100633CO. E.O. acknowledges partial support from the Turkish Academy of Sciences. A.E.S. thanks Dr. T. Magath and Dr. A. Yu. Petrov for the fruitful discussions.

AUTHOR DECLARATIONS

Conflict of Interest

The authors have no conflicts to disclose.

DATA AVAILABILITY

The data that support the findings of this study are available from the corresponding author upon reasonable request.

REFERENCES

- ¹D. Maystre, *Opt. Express* **8**, 209–216 (2001).
- ²S. Collardey, A.-C. Tarot, P. Pouliguen, and K. Mahdjoubi, *Microwave Opt. Technol. Lett.* **44**, 546–550 (2005).
- ³A. E. Serebryannikov, T. Magath, and K. Schuenemann, *Phys. Rev. E* **74**, 066607 (2006).
- ⁴A. Mandatori, M. Bertolotti, and C. Sibilìa, *J. Opt. Soc. Am. B* **24**, 685–690 (2007).
- ⁵A. E. Serebryannikov, K. B. Alici, T. Magath, A. O. Cakmak, and E. Ozbay, *Phys. Rev. A* **86**, 053835 (2012).
- ⁶A. E. Serebryannikov, E. Colak, T. Magath, and E. Ozbay, *J. Opt. Soc. Am. A* **33**, 2450–2458 (2016).
- ⁷P. Rodriguez-Ulbarri, M. Beruete, M. Navarro-Cia, and A. E. Serebryannikov, *Phys. Rev. B* **88**, 165137 (2013).
- ⁸A. Hessel, J. Schmoys, and D. Tseng, *J. Opt. Soc. Am.* **65**, 380–384 (1975).
- ⁹J. W. Heath and E. V. Jull, *J. Opt. Soc. Am.* **68**, 1211–1217 (1978).
- ¹⁰E. V. Jull, J. W. Heath, and G. R. Ebbeson, *J. Opt. Soc. Am.* **67**, 557–559 (1977).
- ¹¹W. Chen, N. C. Beaulieu, D. G. Michelson, and E. V. Jull, *IEEE Trans. Ant. Propag.* **61**, 2342–2347 (2013).
- ¹²M. Memarian, X. Li, Y. Morimoto, and T. Itoh, *Sci. Rep.* **7**, 42286 (2017).
- ¹³C. Ribot, M. S. L. Lee, S. Collin *et al.*, *Adv. Opt. Mater.* **1**, 489–493 (2013).
- ¹⁴O. Hemmatyar, M. A. Abbassi, B. Rahmani, and M. Memarian, *IEEE Trans. Ant. Propag.* **69**, 379–386 (2021).
- ¹⁵A. E. Serebryannikov, Ph. Lalanne, A. Y. Petrov, and E. Ozbay, *Opt. Lett.* **39**, 6193–6196 (2014).
- ¹⁶J. Jung, H. Park, J. Park, T. Chang, and J. Shin, *Nanophotonics* **9**, 3165–3196 (2020).
- ¹⁷J. R. Cheng, S. Inampudi, and H. Mosallaei, *Sci. Rep.* **7**, 12228 (2017).
- ¹⁸M. Aalizadeh, A. E. Serebryannikov, E. Ozbay, and G. A. E. Vandenbosch, *Nanophotonics* **9**, 4589–4600 (2020).
- ¹⁹J. Luan, S. Yang, D. M. Liu, and M. M. Zhang, *Opt. Express* **28**, 3732–3744 (2020).
- ²⁰H. Kwon, E. Arbabi, S. M. Kamali, M. S. Faraji-Dana, and A. Faraon, *Nat. Photon.* **14**, 109–114 (2020).
- ²¹A. E. Serebryannikov, A. O. Cakmak, and E. Ozbay, *Opt. Express* **20**, 14980–14990 (2012).
- ²²D. Sell, J. Yang, S. Doshay, and J. A. Fan, *Adv. Opt. Mater.* **5**, 1700645 (2017).
- ²³V. Vashistha, M. Krawczyk, A. E. Serebryannikov, and G. A. E. Vandenbosch, *Opt. Lett.* **44**, 4725–4728 (2019).
- ²⁴X. Wang, J. Ding, B. Zheng, S. An, G. Zhai, and H. Zhang, *Sci. Rep.* **8**, 1876 (2018).
- ²⁵Z.-L. Deng, Y. Cao, X. Li, and G. P. Wang, *Photon. Res.* **6**, 443–450 (2018).
- ²⁶T. Cai, G.-M. Wang, H.-X. Xu, S.-W. Tang, H. Li, and J.-G. Liang, *Ann. Phys. (Berlin)* **530**, 1700321 (2017).
- ²⁷T. Cai, S. Tang, G. Wang, H. Xu, S. Sun, Q. He, and L. Zhou, *Adv. Opt. Mater.* **5**, 1600506 (2017).
- ²⁸D. Wen, F. Yue, G. Li *et al.*, *Nat. Commun.* **6**, 8241 (2015).
- ²⁹M. Mutlu, S. Cakmakcayan, A. E. Serebryannikov, and E. Ozbay, *Phys. Rev. B* **87**, 205123 (2013).
- ³⁰E. Colak, A. E. Serebryannikov, P. V. Usik, and E. Ozbay, *J. Appl. Phys.* **119**, 193108 (2016).
- ³¹N. Mahmood, I. Kim, M. Q. Mehmood *et al.*, *Nanoscale* **10**, 18323–18330 (2018).
- ³²M. Veysi, C. Guclu, O. Boyraz, and F. Capolino, *J. Opt. Soc. Am. B* **32**, 318–323 (2015).
- ³³M. Ayre, T. J. Karle, L. Wu, T. Davies, and T. F. Krauss, *IEEE J. Select. Areas Commun.* **23**, 1390–1395 (2005).
- ³⁴J. Shi, M. E. Pollard, C. A. Angeles, R. Chen, J. C. Gates, and M. D. B. Charlton, *Sci. Rep.* **7**, 1812 (2017).
- ³⁵A. E. Serebryannikov, A. Y. Petrov, and E. Ozbay, *Appl. Phys. Lett.* **94**, 181101 (2009).
- ³⁶K. Staliunas and V. J. Sánchez-Morcillo, *Phys. Rev. A* **79**, 053807 (2009).
- ³⁷A.-L. Fehrembach, A. Talneau, O. Boyko, F. Lemarchand, and A. Sentenac, *Opt. Lett.* **32**, 2269–2271 (2007).
- ³⁸R. Rabaday and I. Avrutsky, *Opt. Lett.* **29**, 605–607 (2004).
- ³⁹W.-N. Liu, R. Chen, W.-Y. Shi, K.-B. Zeng, F.-L. Zhao, and J.-W. Dong, *Nanophotonics* **9**, 3443–3450 (2020).
- ⁴⁰Z.-L. Deng, S. Zhang, and G. P. Wang, *Opt. Express* **24**, 23118–23128 (2016).
- ⁴¹Y. J. Lee, J. Yeo, R. Mittra, and W. S. Park, *IEEE Trans. Ant. Propag.* **53**, 224–235 (2005).
- ⁴²H. Tanaka, I. Takai, H. Fujikawa, and H. Iizuka, *J. Lightwave Technol.* **36**, 2517–2523 (2018).
- ⁴³Q. Qian, S. Ti, and C. Wang, *Opt. Lett.* **44**, 3984–3987 (2019).
- ⁴⁴S. Gawali, D. Gailevičius, G. Garre-Werner, V. Purlys, C. Cojocaru, J. Trull, J. Montiel-Ponsoda, and K. Staliunas, *Appl. Phys. Lett.* **115**, 141104 (2019).
- ⁴⁵A. Y. Piggott, J. Lu, K. G. Lagoudakis, J. Petykiewicz, T. M. Babinec, and J. Vuckovic, *ACS Photon.* **5**, 301–305 (2018).
- ⁴⁶C. Jin, S. Fan, S. Han, and D. Zhang, *IEEE J. Quant. Electron.* **39**, 160–165 (2003).
- ⁴⁷T. Matsumoto, S. Fujita, and T. Baba, *Opt. Express* **13**, 10768–10776 (2005).
- ⁴⁸M. Koshiba, *J. Lightwave Technol.* **19**, 1970–1975 (2001).
- ⁴⁹S. Pahlavan and V. Ahmadi, *IEEE Photon. Technol. Lett.* **29**, 511–514 (2017).
- ⁵⁰U. G. Yasa, M. Turduduev, I. H. Giden, and H. Kurt, *J. Lightwave Technol.* **35**, 1677–1683 (2017).
- ⁵¹Y. Shi, D. Dai, and S. He, *IEEE Photon. Technol. Lett.* **19**, 825–827 (2007).
- ⁵²M. Sesay, X. Jin, and Z. Ouyang, *J. Opt. Soc. Am. B* **30**, 2043–2047 (2013).
- ⁵³B. A. Slovick, Y. Zhou, Z. G. Yu, I. I. Kravchenko, D. P. Briggs, P. Moirra, S. Krishnamurthy, and J. Valentine, *Phil. Trans. Royal Soc. A* **375**, 20160072 (2017).
- ⁵⁴A. Ozer, N. Yilmaz, H. Kocer, and H. Kurt, *Opt. Lett.* **43**, 4350–4353 (2018).
- ⁵⁵J. Zheng, C. Zhou, J. Feng, H. Cao, and P. Lu, *Opt. Commun.* **282**, 3069–3075 (2009).
- ⁵⁶J. Feng, C. Zhou, J. Zheng, H. Cao, and P. Lv, *Appl. Opt.* **48**, 2697–2701 (2009).
- ⁵⁷D. Ott, I. Divliansky, B. Anderson, G. Venus, and L. Glebov, *Opt. Express* **21**, 29620–29627 (2013).
- ⁵⁸S. Breer and K. Buse, *Appl. Phys. B* **66**, 339–345 (1998).
- ⁵⁹T. Magath and A. E. Serebryannikov, *J. Opt. Soc. Am. A* **22**, 2405–2418 (2005).
- ⁶⁰M. Gumus, I. H. Giden, and H. Kurt, *Opt. Lett.* **43**, 2555–2558 (2018).
- ⁶¹S. Nojima and T. Mizoi, *Phys. Rev. B* **71**, 193106 (2005).

- ⁶²M. Noori, M. Soroosh, and H. Baghban, *Ann. Phys. (Berlin)* **530**, 1700049 (2018).
- ⁶³M. Lester, D. C. Skigin, and R. A. Depine, *Appl. Opt.* **47**, 1711–1717 (2008).
- ⁶⁴M. Lester, D. C. Skigin, and R. A. Depine, *J. Opt. A: Pure Appl. Opt.* **11**, 045705 (2009).
- ⁶⁵Y. Jin and S. He, *Phys. Rev. B* **75**, 195126 (2007).
- ⁶⁶A. F. Peterson, S. L. Ray, and R. Mittra, *Computational Methods for Electromagnetics* (IEEE Press, 1998).
- ⁶⁷*Electromagnetic Theory of Gratings*, edited by R. Petit (Springer, Berlin, 1980).
- ⁶⁸P.-Y. Wang, R. Herrero, M. Botey, Y.-C. Cheng, and K. Staliunas, *Phys. Rev. A* **102**, 013517 (2020).
- ⁶⁹L. Maigyte and K. Staliunas, *Appl. Phys. Rev.* **2**, 011102 (2015).
- ⁷⁰A. Arbabi, E. Arbabi, Y. Horie, S. M. Kamali, and A. Faraon, *Nat. Photon.* **11**, 415–420 (2017).
- ⁷¹Y. G. Ma, C. K. Ong, T. Tyc, and U. Leonhardt, *Nat. Mater.* **8**, 639–642 (2009).
- ⁷²Q. Wang, L. Zhou, P. Wan *et al.*, *Opt. Express* **28**, 30606–30615 (2020).
- ⁷³M. M. Beaky, J. B. Burk, H. O. Everitt, M. A. Haider, and S. Venakides, *IEEE Trans. Microwave Theory Tech.* **47**, 2085–2091 (1999).
- ⁷⁴X. Chen, C. Chardin, K. Makles, C. Caër, S. Chua, R. Braive, I. Robert-Philip, T. Briant, P.-F. Cohadon, A. Heidmann, T. Jacqmin, and S. Deléglise, *Light Sci. Appl.* **6**, e16190 (2017).
- ⁷⁵*Photonic Crystals: Advances in Design, Fabrication, and Characterization*, edited by K. Busch, S. Lölkes, R. B. Wehrspohn, and H. Föll (Wiley, 2006).
- ⁷⁶*Photonic Crystals: Physics, Fabrication and Applications*, edited by K. Inoue and K. Ohtaka (Springer, Berlin, 2004).